Journal of Photochemistry and Photobiology A: Chemistry 305 (2015) 1–10

Contents lists available at ScienceDirect

Journal of Photochemistry and Photobiology A: Chemistry

journal homepage: www.elsevier.com/locate/jphotochem

Ruthenium complexes of ferrocene mannich bases: DNA/BSA interactions and cytotoxicity against A549 cell line

Pulipaka Ramadevi [a], Rinky Singh [a], Sarmita S. Jana [b], Ranjitsinh Devkar [b], Debjani Chakraborty [a,*]

[a] Department of Chemistry, Faculty of Science, The M.S. University of Baroda, Vadodara-390002, Gujarat, India
[b] Division of Phytotherapeutics and Metabolic Endocrinology, Department of Zoology, Faculty of Science, The M.S. University of Baroda, Vadodara-390002, Gujarat, India

ARTICLE INFO

Article history:
Received 4 September 2014
Received in revised form 30 January 2015
Accepted 12 February 2015
Available online 25 February 2015

Keywords:
Ferrocenyl mannich base
Ruthenium complexes
DNA/BSA binding interactions
Cytotoxicity
A549 human lung carcinoma
Apoptosis

ABSTRACT

Two different series of ruthenium complexes, ML_3 and MLL'_2 where M = Ru(III)/Ru(II), L = ferrocenyl amino acid mannich base conjugates and L′ = 1,10-phenanthroline have been synthesized and characterized by spectroscopic methods. These ferrocenyl ligands and their ruthenium complexes have been investigated for their interactions with DNA and BSA (bovine serum albumin) employing steady-state fluorescence quenching measurements, UV–vis spectroscopy and DNA viscosity measurements. High binding constants obtained from the DNA binding studies ($K_b = 10^4 - 10^6\ M^{-1}$) prompted the *in-vitro* cytotoxicity assay of complexes on A549 human lung carcinoma cells (employing MTT assay). The IC_{50} values (within the range of 46 μM–422 μM) obtained herein were found to be lower than those of the well known ruthenium complex NAMI-A currently under phase II clinical trials which has IC_{50} values in the range of 550 μM–750 μM for various cancer cell lines. Interaction of these complexes with A549 cells has been further scrutinized using acridine orange (AO)/ethidium bromide (EB) dual staining technique to indicate apoptosis as the mode of cell death.

1. Introduction

Ferrocene is one of the members of the well known organometallic family- "metallocenes" in which an iron atom is flanked by two cyclopentadienyl (Cp) rings. The unique structural and conformational properties of ferrocene, an atomic ball bearing character, are characterized by the parallel alignment of the two cyclopentadienyl rings and the free rotation of the rings around the axis penetrating their centers. Its remarkable stability and fascinating chemistry has attracted the attention of the scientific and technical community. Owing to the favorable electronic properties of ferrocene and its easy functionalization their applications have been explored in a wide range of scientific areas ranging from catalysis to the design of new nonlinear optic materials to new biologically active compounds. Several structural modifications of established drugs with ferrocenyl moiety have been reported, such as ferrocene fluconazole [1], ferrocene aspirin [2], mefloquine [3] and artemisinin [4]. Moreover ferrocene derivatives have been used as scaffolds to design new molecules that recognize cations, anions, organic molecules, nucleoba-ses, dinucleotides and amino acids [5–10]. Seio et al. [11] have reported new DNA binding molecules utilizing structural and conformational properties of ferrocene. Their design concept is based on the fact that the distance between the two cyclopentadienyl rings of ferrocene, ca. 3.3 Å is close to the distance between two aromatic rings stacked with each other. In addition, it is well-known that the minor groove of DNA can accommodate stacked aromatic rings, as established by the structural studies of natural or synthetic molecules that recognize the minor groove. Therefore, it was expected that ferrocene derivatives could be a new type of DNA binding molecules if appropriately designed aromatic rings were attached to the Cp rings. Recent studies on interaction of ferrocenyl ligands with DNA has shown binding constants to be in the order of 10^3–10^5 [12] agreeing with the above mentioned fact. The stability of ferrocene in aqueous and aerobic media has made ferrocenyl compounds very popular molecules for such biological applications. Furthermore such favorable characteristics of ferrocene led to the design of ferrocenyl derivatives that function as highly

* Corresponding author. Tel.: +91 9537521703.
E-mail address: debchak23@gmail.com (D. Chakraborty).

http://dx.doi.org/10.1016/j.jphotochem.2015.02.010
1010-6030/

sensitive detectors of proteins or as reporters of protein activity. Studies on ferrocenyl conjugates with amino acids and end-labeled ferrocenyl di- and tripeptides have demonstrated distinctive electrical, structural, and medicinal properties [13]. Many researchers have shown interest in design of unnatural ferrocenyl amino acids and peptides which further have been studied for their biomedical applications. Modification of proteins by incorporating such unnatural ferrocenyl amino acids helps the study of protein structure, activity and interaction with other biomolecules [14].

The ferrocenyl compounds are known to hold good potential as anticancer agents. This can be exemplified by the results obtained by the group of Gérard Jaouen, with the development of ferrocifens (*i.e.*, ferrocene-modified tamoxifens), which exhibit strong anti-proliferative effects not only in hormone dependent but also in hormone-independent breast cancer cells [15]. A recent review by Ornelas throws light on the various applications of ferrocene and its derivatives in cancer research [16].

Here we are reporting a series of amino acid conjugated ferrocene mannich bases. These ferrocenyl amino acids have been targeted as it has been shown that tethering biologically active groups to the ferrocenyl unit increases their potency, possibly due to the combined action of the organic molecule with Fenton chemistry of the Fe-center [17,18]. Since DNA represent very important potential target of cancer diagnostic and chemotherapy drugs, before going to expensive cell line study it was decided to preliminarily explore the anticancer potency of the compounds by determining their DNA interaction because 'The control over DNA can control the cancerous cell growth'. Like DNA, proteins are also considered to be one of the prime molecular targets for diagnostic and imaging agents, and so equal attention has been paid on designing novel probes for proteins [19–21].

Several ruthenium compounds have been shown to inhibit DNA replication, possess mutagenic activity, induce SOS repair, and reduce RNA synthesis, which are all consistent with DNA binding of these compounds *in vivo*. Thus, by analogy to platinum antitumor drugs, DNA interactions of antitumor ruthenium agents are of a great interest [22,23].

Complexes of 1,10-phenanthroline (phen) have been shown to exhibit interesting clinical activities including antitumoural, antimycobacterial, antifungal and antimicrobial activities. Moreover, these compounds can be used as DNA intercalating agents and metal synthetic nucleases [24].

The ferrocene amino acid derivatives have been coordinated to Ru^{3+} and $[Ru(phen)_2]^{2+}$ and investigated for their interaction with DNA and bovine serum albumin. Results obtained in the DNA binding studies prompted the *in-vitro* cytotoxicity evaluation of ruthenium complexes on A549 human lung carcinoma cells using MTT assay. The interaction of these complexes with A549 cells has been scrutinized using AO/EB staining technique to assess the mechanism of cell death *viz.* apoptotic or necrotic.

2. Experimental

2.1. Reagents and materials

All the chemicals and solvents used for synthesis and characterization of ligands and complexes are of analytical grade and were used as purchased. Ferrocene carboxaldehyde and DAPI stain were purchased from Sigma–Aldrich. Amino acids, CT-DNA, Tri–sodium citrate and EB (ethidium bromide) were purchased from SRL (Sisco Research Laboratory, Mumbai, India). $RuCl_3.3H_2O$ and BSA (bovine serum albumin) were purchased from Hi media. All the solvents used in the present studies were purchased from Merck and are of analytical grade.

2.2. Methods and instrumentation

^1H NMR spectra of the ligands were recorded on Bruker 400 MHz NMR Spectrophotometer. ESI Mass spectra of the ligands and complexes were recorded on Applied Biosystem API 2000

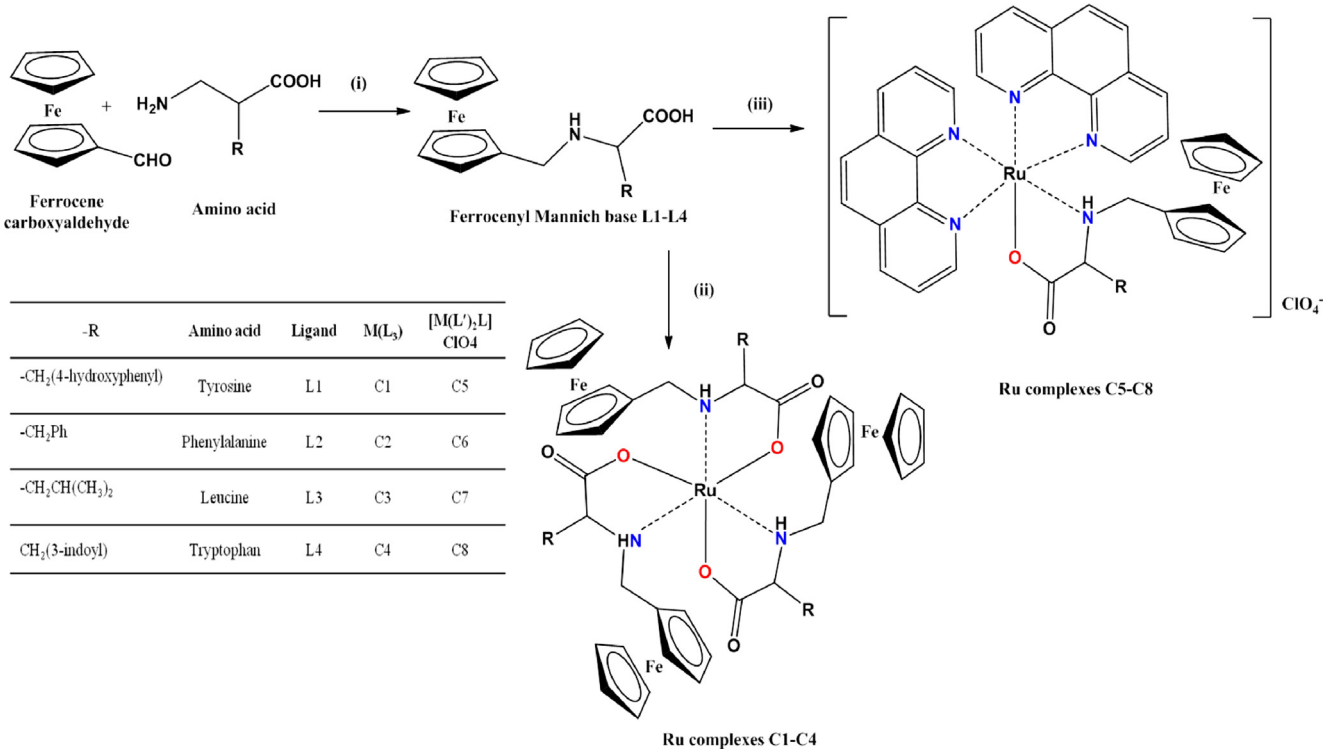

-R	Amino acid	Ligand	$M(L_3)$	$[M(L')_2L]ClO4$
$-CH_2$(4-hydroxyphenyl)	Tyrosine	L1	C1	C5
$-CH_2Ph$	Phenylalanine	L2	C2	C6
$-CH_2CH(CH_3)_2$	Leucine	L3	C3	C7
CH_2(3-indoyl)	Tryptophan	L4	C4	C8

Fig. 1. (i) Dry MeOH, NaOH reflux, $NaBH_4$, stirring at r.t. for 1.5 h, (ii) $RuCl_3.3H_2O$, DMF and reflux for 6 h, (iii) Ru(1,10-phenanthroline)$_2Cl_2$. $2H_2O$, EtOH and reflux for 7 h under N_2.

Mass spectrometer. Infrared spectra (400–4000 cm^{-1}) were recorded on PerkinElmer RX-1 FTIR with samples prepared as KBr pellets. UV spectra were recorded in DMSO solution at concentrations in the range 10^{-6}–10^{-3} M on PerkinElmer Lambda-35 dual beam UV–vis spectrophotometer. C, H and N elemental analysis were performed on a PerkinElmer 240B elemental analyzer. Fluorescence spectra were recorded in solution on JASCO FP-6300 fluorescence spectrophotometer.

2.3. Synthesis of ligands

The ferrocenyl amino acids **L1–L4** were synthesized according to a procedure reported by Goswami et al. [25].

Amino acid (2.76 mmol) and NaOH (2.76 mmol) in dry methanol (5 ml) were stirred for 30 min to get a homogeneous solution. A methanolic solution (5 ml) of ferrocene carboxaldehyde (2.76 mmol) was added dropwise to the above solution, which was refluxed for 90 min, cooled, and treated with sodium borohydride (5.2 mmol) with constant stirring. The solvent was evaporated, the resulting mass was dissolved in water and acidified with dilute HCl, and the solution pH was maintained within 5–6. The ligand that precipitated as a yellow solid was filtered, thoroughly washed with water and cold methanol, and finally dried in vacuum. Yields of all the four ligands **L1–L4** were in the range of 80–90%.

2.4. Synthesis of complexes

2.4.1. $[Ru(L)_3]$

$RuCl_3 \cdot 3H_2O$ (0.2 mmol) and the ferrocenyl ligands (0.6 mmol) were taken in 5 ml DMF and refluxed for 6 h. After reflux the reaction mixture was cooled to r.t. and acetone (5 times the volume of DMF) was added followed by overnight cooling at 0 °C. The brown precipitates of the complexes were then filtered off, washed with acetone and ether and dried in oven at 50 °C. Yields of all the four complexes **C1–C4** were in the range of 50–60%.

2.4.2. $[Ru(L')_2(L)]ClO_4$ (L′ = 1,10-phenanthroline)

$[Ru(L')_2]Cl_2 \cdot 2H_2O$ (0.2 mmol) and the ferrocenyl ligands (0.2 mmol) were taken in 5 ml ethanol and refluxed for 7 h under nitrogen. After reflux the reaction mixture was cooled to r.t. and saturated aqueous solution of sodium perchlorate was added dropwise and stirred for 2 h followed by overnight cooling at 0 °C. The brown precipitates of the complex were then filtered off, washed with water and ether and dried. Yields of all the four complexes **C5–C8** were in the range of 55–60%.

The overall synthetic route of the ligands and complexes has been presented schematically in Fig. 1.

2.5. DNA binding experiments

2.5.1. UV absorption studies

The interaction of compounds with CT DNA has been studied with UV spectroscopy in order to investigate the possible binding modes to CT DNA and to calculate the binding constants (K_b). Absorption studies were performed with fixed compound concentrations while varying the CT-DNA concentration within. Stock solution of the ligands and complexes was diluted with tris buffer to get the desired ligand concentration (75 μM) and complex concentration (37.5 μM–50 μM). While measuring the absorption, equal increments of CT-DNA were added at different ratios to both the compound solution and the reference solution to eliminate the absorbance of CT-DNA itself.

2.5.2. Competitive binding studies with EB using fluorescence spectroscopy

The competitive binding study of each compound with EB has been investigated with fluorescence spectroscopy in order to examine whether the compound can displace EB from DNA–EB complex. The DNA–EB complex was prepared by adding EB (33.3 μM) and DNA (20 μM) in tris buffer. The binding mode of complexes **C5–C8** with CT-DNA was studied by adding a certain amount of a solution of each complex step by step into the solution of the DNA–EB complex. The influence of the addition of each complex has been obtained by recording the variation in the fluorescence emission spectra of the DNA–EB complex. The fluorescence intensities of EB bound to CT-DNA were measured at 609 nm (524 nm excitation) after addition of different concentrations of the complexes at different ratios.

2.5.3. Competitive binding studies with DAPI using fluorescence spectroscopy

The competitive binding study of **C1–C4** with known groove binder DAPI has been investigated with fluorescence spectroscopy. The DNA–DAPI complex was prepared by adding DAPI (5 μM) and DNA (20 μM) in tris buffer. The binding mode of complexes **C1–C4** with CT-DNA was studied by adding a certain amount of a solution of each complex step by step into the solution of the DNA–DAPI complex. The influence of the addition of each complex has been obtained by recording the variation in the fluorescence emission spectra of the DNA–DAPI complex. The fluorescence intensities of DAPI bound to CT-DNA were measured at 451 nm (340 nm

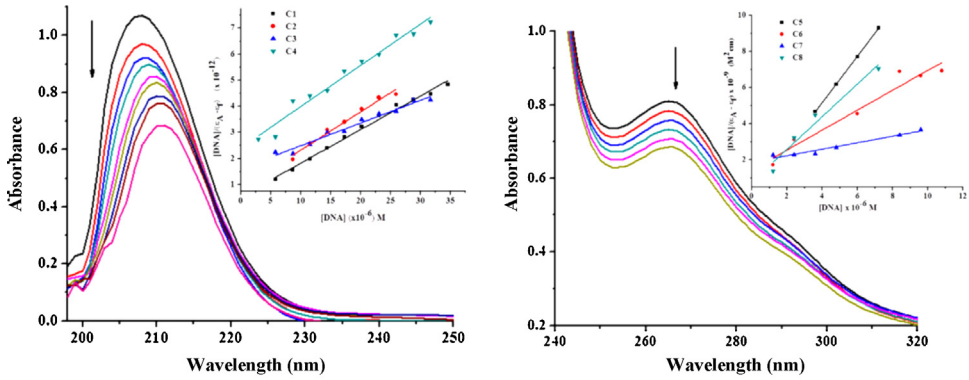

(a) (b)

Fig. 2. Titration plot of complexes (a) **C1** and (b) **C5** with DNA. Insets: Plot of [DNA]/(ε_A–ε_f) *versus* [DNA] for (a) **C1–C4** and (b) **C5–C8**. (For interpretation of the references to color in the text, the reader is referred to the web version of this article.)

excitation) after addition of different concentrations of the complexes at different mixing (r) ratios.

2.5.4. Viscosity measurements

Cannon–Ubbelohde viscometer maintained at a constant temperature of 32.0 ± 0.1 °C in a thermostat was used to measure the relative viscosity of DNA (200 μM) solutions in the presence of complexes **C1–C8** (with [complex]/[DNA] ratio of 0, 0.04, 0.08, 0.12, 0.16, 0.20 and 0.24) in Tris–HCl buffer (pH 7.2). Digital stopwatch with least count of 0.01 s. was used for flow time measurement with accuracy of ±0.1 s. The flow time of each sample was measured three times and an average flow time was calculated. Data are presented as $(\eta/\eta_0)^{1/3}$ *versus* [complex]/[DNA], where η is the viscosity of DNA in the presence of complex and η_0 is the viscosity of DNA alone. Viscosity values were calculated from the observed flow time of DNA-containing solutions (t) corrected for that of the buffer alone (t_0), $\eta = (t - t_0)/t_0$ [26].

2.6. BSA binding experiments

2.6.1. Steady-state fluorescence spectroscopy

The protein-binding study was performed employing steady state fluorescence spectroscopy. Tryptophan fluorescence quenching experiments were carried out using bovine serum albumin (BSA, 8.3 μM) in buffer (containing 15 mM tri-sodium citrate and 150 mM NaCl at pH 7.0). The quenching of emission intensity of the tryptophan residues of BSA at 343 nm was monitored in the presence of increasing concentrations of ligands **L1–L4** (0–166 μM) and complexes **C1–C8** (0–30 μM) as quenchers [27]. Fluorescence spectra were recorded from 300 to 500 nm at an excitation wavelength of 296 nm.

2.7. Cytotoxicity

Standard 3-(4,5-dimethylthiazole)-2,5-diphenyltetraazolium bromide (MTT) assay was used [28]. A549 cells (5.0×10^3 cells well^{-1}) were placed in 96-well culture plates (Tarson India Pvt., Ltd.) and grown overnight at 37 °C in a 5% CO_2 incubator. Compounds to be tested were then added to the wells to achieve final concentrations ranging from 10 to 500 μg/ml. Control wells were prepared by addition of culture medium without the compounds. The plates were incubated at 37 °C in a 5% CO_2 incubator for 24 h. Upon completion of the incubation, MTT dye solution (prepared using serum free culture medium) was added to each well to a final concentration of 0.5 mg/ml. After 4 h of incubation with MTT, the culture media was discarded and the wells were washed with Phosphate Buffer Saline (Hi-Media, India Pvt., Ltd.), followed by addition of DMSO to dissolve the formazan crystals so formed and subsequent incubation for 30 min. The optical density of each well was measured spectrophotometrically at 563 nm using Biotek-ELX800MS universal ELISA reader (Bio-Tek instruments, Inc., Winooski, VT). The IC_{50} values were determined by plotting the percentage viability *versus* concentration on a logarithmic graph and reading off the concentration at which 50% of cells remained viable relative to the control. Each experiment was repeated at least three times to obtain mean values.

Table 1
K_b values of ligands **L1–L4** and their ruthenium complexes **C1–C8**.

Compound	λ_{max}	K_b (M^{-1})
L1	208	6.7×10^4
L2	208	2.6×10^4
L3	209	1.4×10^4
L4	207	1.3×10^4
C1	207	2.4×10^5
C2	208	1.7×10^5
C3	207	5.3×10^4
C4	207	6.6×10^4
C5	264	5.3×10^6
C6	264	3.8×10^5
C7	265	2.5×10^5
C8	266	1.1×10^6

2.8. AO/EB staining technique (induction of apoptosis)

A549 cells were grown in triplicates using a 12 well tissue culture plate and allowed to acclimatize overnight. Next day, cells were treated with **C3** (100 μg/ml) and **C5** (250 μg/ml) and incubated for 16 h. After the incubation, cells were stained with acridine orange and ethidium bromide dyes for 5 min in dark and immediately washed three times with PBS. The cells were then suspended in PBS and photographed on confocal LSM-710 fluorescence microscope [29].

3. Results and discussion

3.1. Characterization

3.1.1. NMR spectroscopy

The ^{1}H NMR spectra of ligands **L3** and **L4** show 9 proton multiplet in the δ range of 4–5 ppm that can be ascribed to the ferrocenyl ring protons. The singlet signals at δ = 1–2 pertains to the N—H and COO—H proton of the amino acid. The spectrum of **L3** (Fig. S1,a), apart from the above mentioned signals, also shows a 6 proton singlet at δ = 1.2 ppm owing to two methyl groups—CH $(CH_3)_2$ of leucine. Whereas the spectrum of **L4** (Fig. S1,b) shows 5 proton multiplet in the δ range of 7–8 ppm ascribable to the aromatic protons of the tryptophan and a one proton singlet at δ = 11 ppm attributed to the indoyl N—H.

3.1.2. Mass spectrometry

The ESI-MS spectra of the ligands **L1–L4** and their complexes **C1–C8** showed molecular ion peaks at m/z values equivalent to their molecular weights. The m/z values of all the complexes are in well agreement with the proposed composition (Fig. 1) and have been tabulated in Table S1. All the mass spectra have been provided as Supplementary material Fig. S2. Furthermore the composition and purity of the complexes have been confirmed by their C, H, N elemental analysis, data of which has been provided in Table S1.

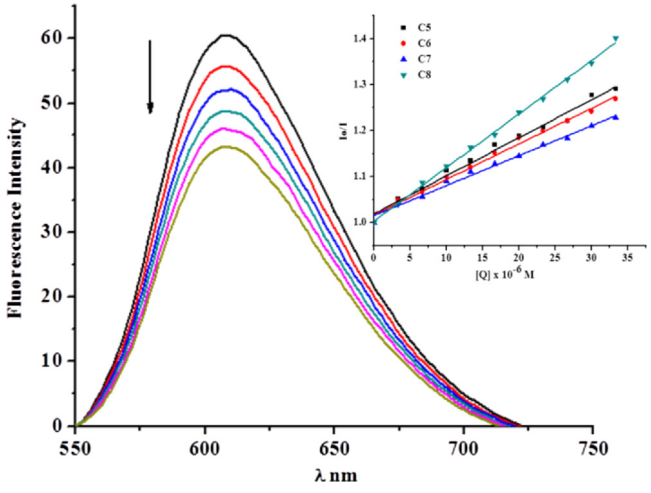

Fig. 3. Plot of Fluorescence emission intensity I *versus* wavelength λ for CT DNA–EB complex at different concentrations of **C5**. Inset: Stern–Volmer quenching plot of CT-DNA–EB for **C5–C8**.

3.1.3. FTIR spectroscopy

The FTIR spectra of the complexes **C1–C8** displayed characteristic strong stretching bands at 1520–1580 cm^{-1} and weaker bands at 1490–1514 cm^{-1} due to asymmetric and symmetric carboxylate (COO^-) stretch respectively which were found as strong bands in the fingerprint region at 1580–1610 cm^{-1} in the spectra of free ligands **L1–L4**. Moreover the distinct broad band at ~3450 cm^{-1} owing to the O—H stretching of free carboxylic acid group found in the ligand is completely lost in the IR spectra of the complex indicating complexation of the ligand with metal *via* the carboxylate oxygen. Furthermore the medium secondary amine N—H stretching bands found in the spectra of the free ligands **L1–L4** in the region of 2900–3000 cm^{-1} was found to have a positive shift in the region of 3080–3200 cm^{-1} in **C1–C8** indicating complexation of the ligand with metal *via* the nitrogen of secondary amine (mannich base). The presence of perchlorate as the counter ion in the complexes **C5–C8** is indicated by its ν_{Cl-O} stretching band in the range of 625–635 cm^{-1} [30]. All the important stretching values have been tabulated in Table S2.

3.1.4. Electronic spectra

The electronic absorption spectra of the ligands **L1–L4** and complexes **C1–C8** in DMSO solution were recorded in the region 200–900 nm. The electronic spectra of free ligands displayed intense absorption bands at 207–209 nm ascribed to π–π^* intra ligand transition of the cyclopentadienyl rings of ferrocene (Fig. S3, a) which were observed unchanged in the spectra of the complexes **C1–C4** (Fig. S3,b). The intra ligand transition bands of complexes **C5–C8** were observed at longer wavelength region at 278–282 nm (Fig. S3,d) due to coordination with Ru(II). In addition all the complexes showed peaks in the region 382–488 nm corresponding to dπ–π^* MLCT transitions (Fig. S3,c and d). Furthermore, complexes **C5–C8** showed Ru(II) centered distinct d–d bands in the visible region 680–700 nm (Fig. S3,d). The absorption peak values have been tabulated in Table S3.

3.2. DNA binding studies

3.2.1. Electronic absorption titration

The presence of ground state interactions between the biological macromolecule DNA and compounds under study have been detected using absorption spectroscopy. DNA can provide three distinctive binding sites (groove binding outside of DNA helix, along major or minor groove, electrostatic binding to phosphate group and intercalation), a behavior important for the biological role of antibiotic and anticancer drugs *in vivo* [31]. The binding efficiency of metal complex to DNA can be effectively investigated employing electronic spectroscopy since the observed changes in the spectra may give evidence of the existing interaction mode [32]. Any interaction between the compounds (**LI–L4** and **C1–C8**) and DNA is expected to perturb the ligand centered transitions of the compounds. Binding with DNA *via* non-intercalative binding modes, such as electrostatic forces, van der Waals interactions, dative bonds, hydrogen bonds and hydrophobic interactions generally results in increase in absorption intensity (hyperchromism) upon increasing the concentration of CT-DNA owing to the degradation of the DNA double helix structure. On the other hand intercalation generally results in hypochromism and a red shift (bathochromism) of the absorption band due to a strong stacking interaction between an aromatic moiety of the ligand and the base pairs of the DNA [33]. The UV spectra of ligands **L1–L4** (10^{-9} M), complexes **C1–C4** (10^{-9} M) and **C5–C8** (10^{-6} M) have been recorded in absence and presence of varying CT-DNA concentration ($1–50 \times 10^{-6}$ M) within. The absorption bands of the ligands **L1–L4** (Fig. S4) and complexes **C1–C4** (Fig. 2a) centered at 207–208 nm showed significant hypochromism and a slight red shift, speculative of primarily groove binding nature of the compounds whereas the absorption bands of complexes **C5–C8** (Fig. 2b) centered at 264–266 nm also exhibited hypochromism but with negligible red shift. DNA intercalators show a much larger bathochromic shift and hypochromism of the spectral bands, although the intercalative mode of binding of the complexes with DNA cannot be ruled out completely [25].

The magnitude of binding strength to CT-DNA may be determined through the calculation of binding constant K_b which is obtained by monitoring the changes in the absorbance of the compounds with increasing concentrations of CT-DNA. K_b is given by the ratio of slope to the *y* intercept in plots [DNA]/(ε_A–ε_f) versus [DNA] (Fig. 2, insets*)* according to Eq. (1) [34]

$$\frac{[DNA]}{(\varepsilon_A - \varepsilon_f)} = \frac{[DNA]}{(\varepsilon_b - \varepsilon_f)} + \frac{1}{K_b(\varepsilon_b - \varepsilon_f)} \quad (1)$$

where [DNA] is the concentration of DNA in base pairs, $\varepsilon_A = A_{obsd}$/[compound], ε_f is the extinction coefficient for the unbound compound (**L1–C8**) and ε_b is the extinction coefficient for the compound in the fully bound form. The binding constant K_b values (Table 1) for the ligands are in the range of 6.7×10^4–1.3×10^4 M^{-1} indicative of strong binding of the ligands with ligand **L1** showing the highest binding constant. The K_b values of metal complexes showed 10–100 folds higher binding efficacy compared to the ligands. In general, complexes **C5–C8** with two 1,10 phenanthroline moieties bound to the metal center, exhibit stronger binding interactions (10^5–10^6 M^{-1}) than complexes **C1–C4** (10^4–10^5 M^{-1}) due to (i) intercalation facilitated by the presence of phenanthroline ligands by insertion of the complex into the adjacent base pairs of DNA and (ii) groove binding of the ferrocenyl moiety. Complex **C5** with a tyrosine substituted ferrocenyl moiety bound to the Ru (II) center shows the highest binding constant value due to additional hydrogen bonding interactions between —OH group of tyrosine and DNA nucleobases which are accessible both in major groove and minor groove and is also observed in the case of the free ligand **L1**. Complex **C8** with a tryptophan substituted ferrocenyl moiety bound to Ru(II) center shows a similar binding constant value as **C5** which also may be due to additional hydrogen bonding interaction between —NH group of tryptophan and DNA nucleobases. The titration curves for ligands **L1–L4**, complexes **C2–C4** and **C6–C8**, as well as Plot of [DNA]/(ε_A–ε_f) *versus* [DNA] for **L1–L4** have been provided as Supplementary material in Fig. S4.

3.2.2. Competitive binding studies with ethidium bromide using fluorescence spectroscopy

To further examine the mode of binding of the compounds with DNA, *via* intercalation or groove binding, a competitive binding study with two dyes: EB and DAPI have been carried out using steady state fluorescence spectroscopy. Ethidium bromide (=3,8-diamino-5-ethyl-6-phenyl-phenanthridinium bromide) is a phenanthridine fluorescence dye and is a typical indicator of intercalation, forming soluble complexes with nucleic acids and emitting intense fluorescence in the presence of CT DNA due to the intercalation of the planar phenanthridinium ring between adjacent base pairs on the double helix [35,36]. Addition of a second molecule, which may bind to DNA more strongly than EB results in a decrease of the DNA-induced EB emission [37]. The

Table 2
K_{SV} values of ruthenium complexes **C5-C8**.

Compound	K_{SV} (M^{-1})
C5	8.3×10^3
C6	7.3×10^3
C7	6.5×10^3
C8	1.2×10^4

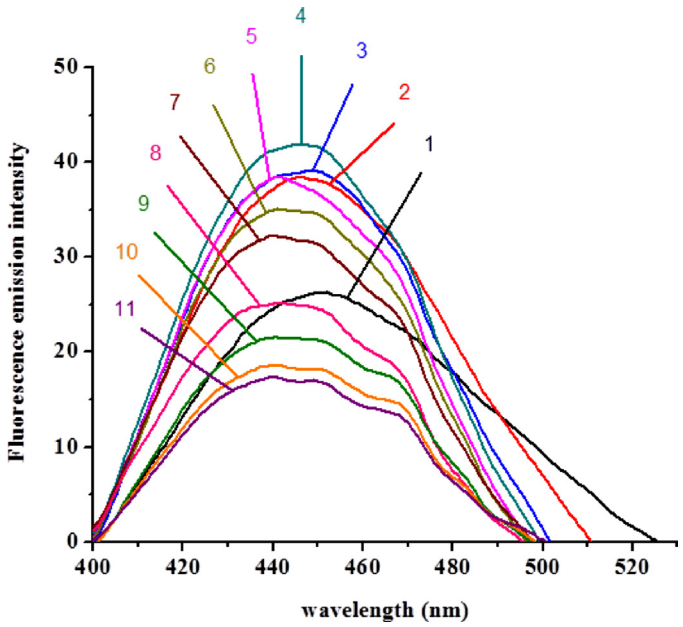

Fig. 4. Plot of DNA-DAPI competitive binding titration curve with **C1**.

emission spectra of DNA–EB (λ_{ex} = 546 nm, λ_{em} = 610) in the absence and presence of increasing amounts of ligands and complexes have been recorded. Addition of the ligands **L1–L4** or the complexes **C1–C4** did not have any kind of effect on the emission intensity or nature of the emission of DNA–EB complex. On the other hand addition of complexes **C5–C8** resulted in a significant decrease of the intensity of the emission band at 609 nm indicating the competition of the compounds with EB in binding to DNA (Fig. 3). The observed quenching of DNA–EB fluorescence suggests that they displace EB from the DNA–EB complex and interact with DNA by intercalation. The planar phenanthroline ligands of complexes **C5–C8** seems to have facilitated intercalation resulting in partial replacement of EB from DNA–EB complex resulting in the observed quenching of fluorescence.

The relative binding of complexes to CT-DNA was determined by calculating the quenching constant (K_{SV}) from the slopes of straight lines obtained from the Stern–Volmer Eq. (2) [38]:

$$\frac{I_0}{I} = 1 + K_{sv}[Q] \quad (2)$$

where I_0 and I are the emission intensities in the absence and the presence of the quencher (**C5–C8**) respectively, [Q] is the concentration of the quencher and K_{SV} is the Stern–Volmer constant which can be obtained from the slope of the plot of I_0/I *versus* [Q].

The Stern–Volmer quenching plots (Fig. 3, inset) illustrate that the quenching of EB bound to DNA by **C5–C8** is in good agreement (R = 0.93–0.99) with the linear Stern–Volmer equation and the

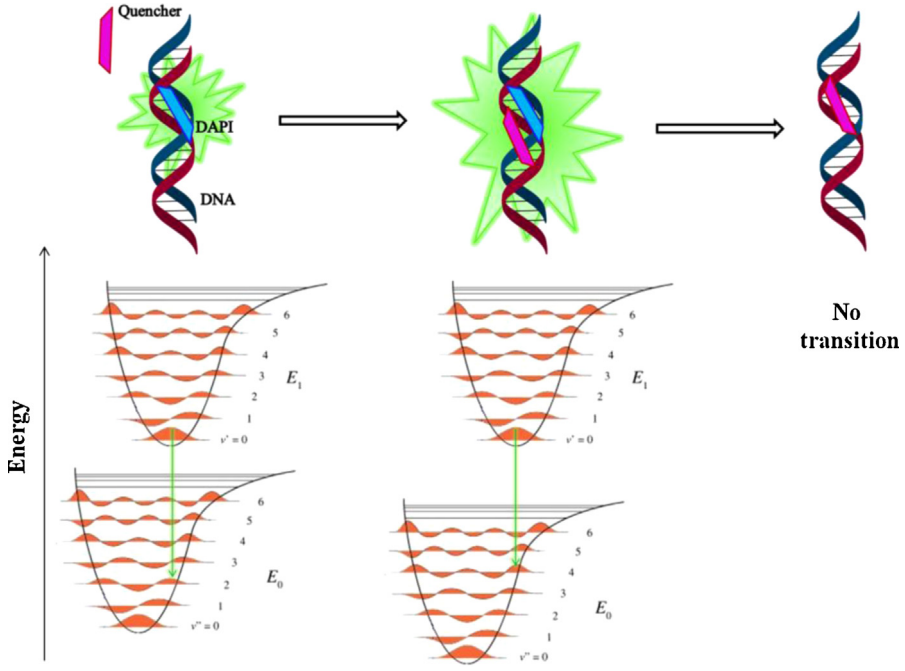

Fig. 5. Schematic presentation of DAPI displacement from DNA helix by quencher molecule followed by fluorescence quenching and corresponding energy diagrams.

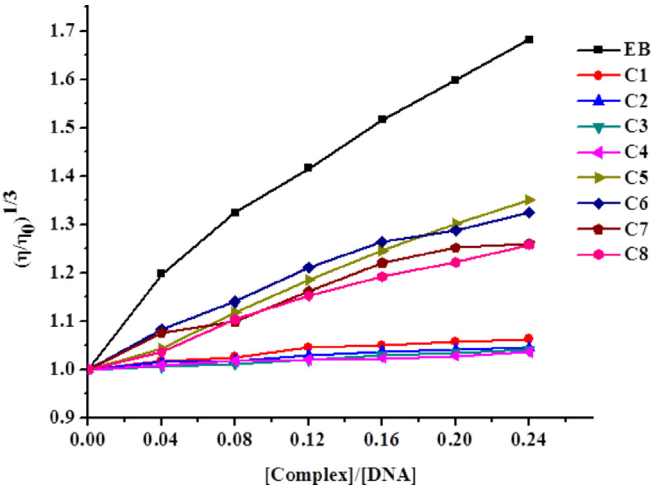

Fig. 6. Effect of increasing amounts of the complexes **C1–C8** and ethidium bromide (EB) on the relative viscosity of CT-DNA (200 μM) in Tris–HCl buffer at 32 (±0.1) °C. [Complex]/[DNA] = 0, 0.04, 0.08, 0.12, 0.16, 0.20 and 0.24.

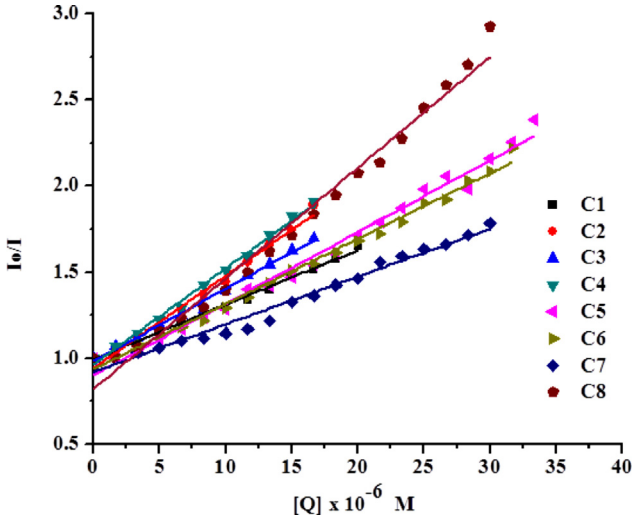

Fig. 8. Stern–Volmer plots for the quenching of BSA fluorescence by **C1–C8**.

Stern–Volmer quenching constant K_{SV} values are given in Table 2. Complexes **C8** and **C5** show higher quenching constant values of $1.2 \times 10^4\,M^{-1}$ and $8.3 \times 10^3\,M^{-1}$ respectively indicating their greater efficiency to replace EB and bind strongly with DNA which is also evident from their higher DNA binding constant (K_b) values. The titration curves for **C6–C8** have been provided as Supplementary material in Fig. S5.

3.2.3. Competitive binding studies with DAPI using fluorescence spectroscopy

DAPI (4′,6-diamidino-2-phenylindole) is a classical minor groove binder to DNA molecule. It is also shown to bind specifically to GC regions by intercalation; however, the minor binding to AT regions is 2 orders of magnitude stronger than the intercalative binding mode. The fluorescence of DAPI increases approximately 30 times when 20-fold excess (base pairs) of DNA is added to the solution of the dye [39,40]. The fluorescence spectra of a mixture of DNA–DAPI solution with increasing concentration of **C1–C4** have been recorded (Fig. 4). The addition of aliquots of the complexes cause an initial slight fluorescence enhancement which on further addition of greater amounts showed subsequent quenching of the DNA–DAPI fluorescence. The initial fluorescence enhancement can be attributed to partial overlap of the electronic states of the quencher molecules (**C1–C4**) and DNA–DAPI complex leading to partial stabilization of the ground state complex and an increase in the value of the Franck–Condon factor. The fluorescence intensity is proportional to the overlap of vibrational wavefunctions and consequently to the Franck–Condon factor. A quencher molecule when approaches a DNA–DAPI complex, it forms an intermediate complex, which is temporarily more stable than the original DNA–DAPI complex. This shifts the ground electronic state to left and down, and as a result the overlap between the vibrational functions in the excited and ground electronic states increases due to the Frank–Condon principle (greater the overlap between the vibrational functions of excited and ground states of the complex, greater is the Franck–Condon factor), leading to the increase in fluorescence signal. Further addition of the quencher leads to the complete displacement of DAPI from the DNA helix and fluorescence depletion [41]. This phenomenon has been explained schematically in Fig. 5. The quenching of the DNA–DAPI fluorescence is conclusive of the fact that complexes **C1–C4** are replacing DAPI from the minor grooves of DNA and themselves getting bound. Moreover a small hump can be seen forming slowly on increasing concentration of the compounds in titration curves 7–11 (Fig. 4) marking the initiation of a new peak formation which is indicative of a ground state complex formation of the compounds with DNA. Thus it can be concluded that complexes **C5–C8** with planar phenanthroline rings, bind to CT-DNA *via* intercalation

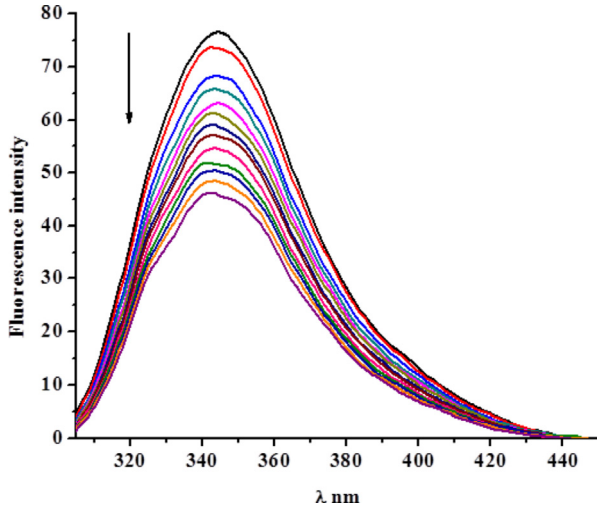

Fig. 7. Plot of Fluorescence emission intensity *versus* wavelength for BSA at different concentrations of **C1**.

Table 3
K_{SV},k_q, K_a and n values for ligands and complexes.

Compound	K_{SV} (M^{-1})	k_q ($M^{-1}\,s^{-1}$)	K_a (M^{-1})	n
L1	4.5×10^3	4.5×10^{11}	1.8×10^3	0.98
L2	4.2×10^3	4.2×10^{11}	1.0×10^3	0.8
L3	2.5×10^3	2.5×10^{11}	1.1×10^3	0.9
L4	8.9×10^3	8.9×10^{11}	3.0×10^3	0.87
C1	3.2×10^4	3.2×10^{12}	5.5×10^4	1.05
C2	5.3×10^4	5.3×10^{12}	8.1×10^5	1.2
C3	4.2×10^4	4.2×10^{12}	5.2×10^4	1.02
C4	5.6×10^4	5.6×10^{12}	2.8×10^5	1.14
C5	4.1×10^4	4.1×10^{12}	2.8×10^6	1.41
C6	3.8×10^4	3.8×10^{12}	7.3×10^6	1.28
C7	2.8×10^4	2.8×10^{12}	5.8×10^6	1.51
C8	6.4×10^4	6.4×10^{12}	9.6×10^6	1.48

Table 4
IC_{50} values of complexes **C1–C8** obtained from MTT assay on A549 cells.

Compound	IC_{50} values	
	(μg/ml)	(μM)
C1	180	145
C2	125	105
C3	50	46
C4	105	80
C5	250	266
C6	390	422
C7	300	337
C8	275	286

whereas complexes **C1–C4** without the phenanthroline rings prefer groove binding.

3.2.4. Viscosity measurements

In order to further confirm the modes of binding of complexes **C1–C8** to CT-DNA, viscosity measurements of DNA solutions were carried out in presence and absence of these complexes. The viscosity of DNA is sensitive to length changes and is regarded as the least ambiguous and the most critical clues of a DNA binding mode in solution [42]. In general, intercalating agents are expected to elongate the double helix to accommodate the ligands in between the base pairs, leading to an increase in the viscosity of DNA. In contrast, a complex that binds exclusively in the DNA grooves typically causes less pronounced (positive or negative) or no changes in DNA solution viscosity [31,43]. The effects of complexes **C1–C8** and classical intercalator EB on the viscosities of CT-DNA solution are shown in Fig. 6. For complexes **C5–C8** with increasing [complex]/[DNA] concentration ratios, the relative viscosities of CT-DNA increased gradually indicative of characteristic intercalative mode of binding which is in accordance with previous findings. In contrast with increasing [complex]/[DNA] concentration ratios for complexes **C1–C4** no significant change in the relative viscosity of CT-DNA solution was observed which ruled out intercalative binding mode of complexes and is consistent with the DNA groove binding as indicated by DNA–DAPI competitive binding studies.

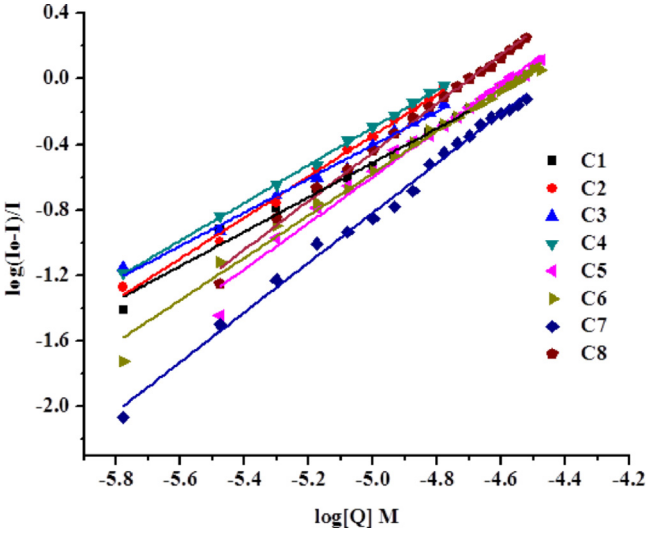

Fig. 9. Double logarithmic plot for the quenching of BSA fluorescence by **C1–C8**.

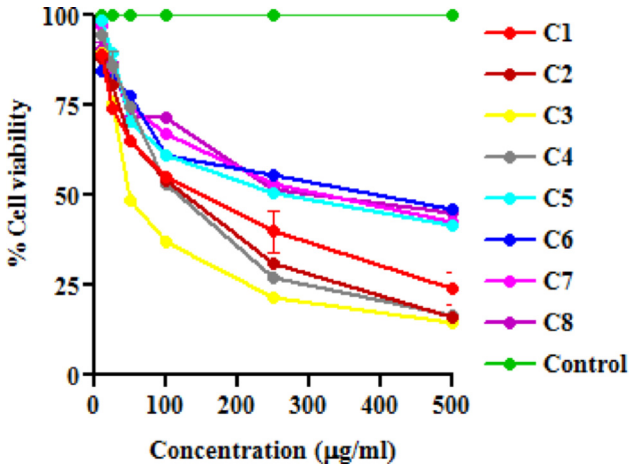

Fig. 10. % Cell viability in presence of complexes **C1–C8** for A549 human lung cancer cell lines. Each point is the mean ± standard error obtained from three independent experiments.

3.3. BSA binding studies

3.3.1. Steady-state fluorescence spectroscopy

BSA is extensively studied, due to its structural homology with human serum albumin (HSA). HSA contains one tryptophan located at position 214, while BSA has two tryptophan residues at positions 134 and 212 along the chain. BSA solutions exhibit a strong fluorescence emission with a peak at 343 nm, due to the tryptophan residues, when excited at 296 nm [44,45]. Neither the ligands nor the complexes show any emission in the range 300–450 nm on excitation at 296 nm. Addition of increasing concentrations of the ligands (**L1–L4)** and complexes (**C1–C8)** to a solution of BSA results in a decrease of the fluorescence intensity as shown for **C5** in Fig. 7 because of their binding to BSA which may change the protein conformation, subunit association or denaturation leading to changes in the tryptophan environment of BSA.

The values of the Stern–Volmer quenching constant ($K_{SV,}$ M^{-1}) and the quenching rate constant (kq, M^{-1} s^{-1}) for the ligands **L1–L4** and the complexes **C1–C8** interacting with BSA as calculated by Stern–Volmer quenching equation (Eq. (2)) and the corresponding Stern–Volmer plots (Fig. 8) are cited in Table 3 which suggest good binding propensity of the complexes with BSA. The K_q values (>10^{11} M^{-1} s^{-1}) are greater than diverse kinds of quenchers for biopolymer fluorescence (10^{10} M^{-1} s^{-1}) indicating the existence of static quenching mechanism [46]. The titration curves for ligands **L1–L4** and complexes **C2–C8** are provided as Supplementary material in Fig. S6 and the Stern–Volmer plots of ligands **L1–L4** are provided as Supplementary material in Fig. S7.

The association binding constant K_a (M^{-1}) and the number of binding sites per albumin (n) can be calculated by double logarithm equation (Eq. (3)) [47]

$$\frac{\log(I_0 - I)}{I} = \log K_a + n\log[Q] \quad (3)$$

The plot of log $[(I_0 - I)/I]$ versus log [Q] for all the ligands and complexes are linear (Fig. 9) and the K_a and n values for ligands **L1–L4** and for complexes **C1–C8** have been obtained from the intercept and slope, respectively (Table 3). The double log plot for ligands **L1–L4** is provided as Supplementary material in Fig. S8.

In general, the values of quenching rate constants (K_q) and association binding constants (K_a) are higher for complexes **C1–C4** as compared to the ligands indicating complexation to ruthenium increases their BSA binding affinities. Additionally higher values for **C5–C8** compared to **C1–C4** reveal that the coordination of

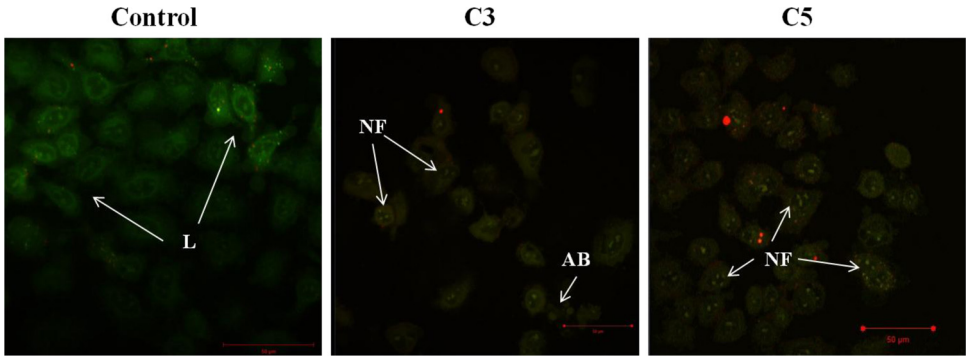

Fig. 11. Confocal images of A549 cells treated with (100 μg/ml) **C3** and (250 μg/ml) **C5** for 16 h followed by dual staining with AO/EB. Here "L" stands for live cells, "NF" stands for nuclear fragmentation and "AB" stands for apoptotic bodies. (For interpretation of the references to color in the text, the reader is referred to the web version of this article.)

ferrocenyl amino acids to ruthenium in the presence of 1,10-phenanthroline leads to enhanced affinity to BSA. The *n* values for the ligands as well as the complexes average out to be 1 which suggests that there is only one binding site available on the protein. Moreover the linear nature of the double logarithm plots of **L1–L4** and **C1–C8** indicates that only one of the tryptophan residues on BSA protein is interacting with the compounds [48].

3.4. Cytotoxicity

In-vitro cytotoxicity tests were performed on the human lung carcinoma (A549) cell line. The cell viabilities (%), obtained for A549 cells with continuous exposure to the compounds for 24 h, are depicted in Fig. 10. The cytotoxicities of the complexes were found to be dose dependent, that is, the cell viability decreased with increasing concentrations. The IC_{50} values of the complexes have been tabulated in Table 4. The reported IC_{50} values of NAMI-A which is a well known ruthenium complex currently under phase 2 clinical trials is in the range of 550 μM–750 μM for various cancer cell lines [49]. Although the synthesized ruthenium complexes are found to be less active compared to *cis* platin (IC_{50} = 26 μM), they are much more active on A549 cancer cells as compared to NAMI-A with complex **C3** (IC_{50} = 46 μM) showing the maximum potency.

Experimental data on NAMI-A and Keppler like complexes have led to the proposal that Ru(III) complexes are, in fact, prodrugs that act by an "activation by reduction" mechanism, yielding more active Ru(II) species. By analogy, lower IC_{50} values of **C1–C4** as compared to **C5–C8** may be due to their reduction to active Ru(II) species in the hypoxic medium within the tumor cells. Alternatively the high anticancer activity of **C1–C4** may be due to the presence of more number of ferrocene moieties which are known to have good anticancer activity [15,16,50]. The *in-vitro* anticancer activity of the compounds was inconsistent with their DNA-binding abilities. The complexes with only ferrocenyl ligands (**C1–C4)** were found to be more cytotoxic than the complexes with both ferrocenyl and phenanthroline ligands (**C5–C8)**, whereas the DNA binding order is the reverse *i.e.*, **C5–C8** > **C1–C4**. The different order of DNA binding affinity and the *in-vitro* anticancer activity means multiple targets and multiple mechanisms coexisted in the anticancer process of the compounds. DNA binding and cleavage need not be the only target and mechanism for cytotoxicity [51].

3.5. Induction of apoptosis

DNA-binding dyes AO and EB (Sigma, USA) were used for the morphological detection of apoptotic and necrotic cells. Acridine orange (AO) permeates all cells and makes the nuclei appear green. Ethidium bromide (EB) is only taken up by cells when cytoplasmic membrane integrity is lost, and stains the nucleus red. EB also dominates over AO. Thus live cells have a normal green nucleus; early apoptotic cells have bright green nucleus with condensed or fragmented chromatin; late apoptotic cells display condensed and fragmented orange chromatin; cells that have died from direct necrosis have a structurally normal orange nucleus [52]. The cells were treated with **C3** at 100 μg/ml and with **C5** at 250 μg/ml concentration for 16 h. The confocal images of control cells show that the live cells are stained with AO and hence emit green fluorescence whereas the treated cells bearing yellow nucleus indicating early apoptosis (Fig. 11). Moreover distinct nuclear fragmentation can also be seen within the treated cells and the presence of apoptotic bodies makes it evident that the mode of cell death is apoptosis.

4. Conclusion

The work discussed here thus focuses on the synthesis, characterization and bioactivity of ferrocenyl amino acid mannich base conjugates and their ruthenium complexes of: (1) $M(L)_3$ type where M = Ru(III), L = ferrocenyl amino acid mannich base conjugates and (2) $M(L')_2L$ type where M = Ru(II), L′ = 1,10-phenanthroline. Literature has already shown that ferrocenyl compounds are good DNA and protein binders which in the present study have been found to be further enhanced on complexation with ruthenium. This can be based on their better binding constants obtained for interactions with DNA and BSA compared to those of the free ligands. Moreover the ferrocenyl mannich base ligands and their ML_3 type Ru(III) complexes have been found to be good groove binders unlike their mixed ligand Ru(II) complexes which show intercalative mode of binding to DNA. Such impressive binding efficacies of the ruthenium complexes containing ferrocenyl amino acids broaden their scope for *in-vitro* investigations as potent anticancer agents following which we carried out the cytotoxicity studies employing MTT assay. Lower IC_{50} values of the Ru(III) complexes, **C1–C4** can be either attributed to their reduction to active Ru(II) species in the hypoxic medium within the tumor cells or to the presence of three ferrocene moieties which have been shown to be active against tumor cells. Furthermore the mode of cell death, scrutinized using AO/EB dual staining technique was found to be apoptosis also called as programmed cell death which is the preferred mode of cell death over necrosis.

Acknowledgements

The authors gratefully acknowledge the University Grants Commission RFSMS-BSR fellowship [UGC No. F.4-1/2006 (BSR)/5-

68/2007 (BSR)], New Delhi, for their financial assistance. The authors are thankful to the Head, Department of Chemistry and Department of Zoology, Faculty of Science, The Maharaja Sayajirao University of Baroda for providing us with the necessary lab facilities and required instrumentation facilities to carry out the research work. Thanks are also due to Dr. M.N. Patel, Department of Chemistry, Sardar Patel University, Vidyanagar for the DNA viscosity measurements. The authors thank DBT-MSUB-ILSPARE project, Dr. Vikram Sarabhai Science Block, M.S.University of Baroda for providing the confocal LSM-710 fluorescence microscope in order to procure the confocal images of AO/EB staining technique.

Appendix A. Supplementary data

Supplementary data associated with this article can be found, in the online version, at http://dx.doi.org/10.1016/j.jphotochem.2015.02.010.

References

[1] B. Christophe, F. Nadine, M. Lucien, B. Jacques, P. Daniel, Bioorg. Med. Chem. Lett. 10 (2000) 839–841.
[2] R. Epton, G. Marr, G.K. Rogers, J. Organomet. Chem. 110 (1976) 42–44.
[3] B. Christophe, D. Laurence, A.M. Lucien, M. Marlène, C. Daniel, S.B. Jacques, Eur. J. Med. Chem. 35 (2000) 707–714.
[4] B. Francois, C. Frederic, V. Laure, B. Jacques, M. Bernard, R. Anne, J. Med. Chem. 53 (2010) 4103–4109.
[5] A. Ion, J. Moutet, E. Saint-Aman, G. Royal, I. Gautier- Luneau, M. Bonin, R. Ziessel, Eur. J. Inorg. Chem. 6 (2002) 1357–1366.
[6] L.J. Kuo, J.H. Liao, C.T. Chen, C.H. Huang, C.S. Chen, J.M. Fang, Org. Lett. 5 (2003) 1821–1824.
[7] J. Westwood, S.J. Coles, S.R. Collinson, G. Gasser, S.J. Green, M.B. Hursthouse, M.E. Light, J.H. Tucker, Organometallics 23 (2004) 946–951.
[8] M. Inouye, Y. Hyodo, H. Nakazumi, J. Org. Chem. 64 (1999) 2704–2710.
[9] M. Takase, M. Inouye, J. Org. Chem. 68 (2003) 1134–1137.
[10] P. Debroy, M. Banerjee, M. Prasad, S.P. Moulik, S. Roy, Org. Lett. 7 (2005) 403–406.
[11] K. Seio, M. Mizuta, T. Terada, M. Sekine, J. Org. Chem. 70 (2005) 10311–10322.
[12] (a) R. Gul, M.K. Rauf, A. Badshah, S.S. Azam, M.N. Tahir, A. Khan, Eur. J. Med. Chem. 85 (2014) 438–449;
(b) S. Hussain, A. Badshah, B. Lal, R.A. Hussain, S. Ali, M.N. Tahir, A.A. Altaf, J. Coord. Chem. 67 (2014) 2148–2159;
(c) T.K. Goswami, S. Gadadhar, M. Roy, M. Nethaji, A.A. Karande, A.R. Chakravarty, Organometallics 31 (2012) 3010–3021.
[13] A.M. Gellett, P.W. Huber, P.J. Higgins, J. Organomet. Chem. 693 (2008) 2959–2962.
[14] P.J. Higgins, A.M. Gellett, Bioorg. Med. Chem. Lett. 19 (2009) 1614–1617.
[15] (a) S. Top, A. Vessières, G. Leclercq, J. Quivy, J. Tang, J. Vaissermann, M. Huché, G. Jaouen, Chem. A Eur. J. 9 (2003) 5223–5236;
(b) G. Jaouen, S. Top, A. Vessières, G. Leclercq, M.J. McGlinchey, Curr. Med. Chem. 11 (2004) 2505–2517;
(c) A. Vessières, S. Top, P. Pigeon, E. Hillard, L. Boubeker, D. Spera, G. Jaouen, J, . Med. Chem. 48 (2005) 3937–3940;
(d) E. Hillard, A. Vessières, L. Thouin, G. Jaouen, C. Amatore, Angew. Chem. Int. Ed. 45 (2006) 285–290;
(e) A. Vessieres, S. Top, W. Beck, E. Hillard, G. Jaouen, Dalton Trans. (2006) 529e541;
(f) A. Nguyen, E.A. Hillard, A. Vessières, S. Top, P. Pigeon, G. Jaouen, Chimia 61 (2007) 716–724;
(g) O. Buriez, J.M. Heldt, E. Labbé, A. Vessières, G. Jaouen, C. Amatore, Chem. A Eur. J. 14 (2008) 8195–8203;
(h) Q. Michard, G. Jaouen, A. Vessieres, B.A. Bernard, J. Inorg. Biochem. 102 (2008) 1980–1985;
(i) P. Pigeon, S. Top, O. Zekri, E.A. Hillard, A. Vessières, M.-A. Plamont, O. Buriez, E. Labbé, M. Huché, S. Boutamine, C. Amatore, G. Jaouen, J. Organomet. Chem. 694 (2009) 895–901;
(j) M. Gormen, D. Plazuk, P. Pigeon, E.A. Hillard, M.-A. Plamont, S. Top, A. Vessières, G. Jaouen, Tetrahedron Lett. 51 (2010) 118–120.
[16] C. Ornelas, New J. Chem. 35 (2011) 1973–1985.
[17] J. Prousek, Pure Appl. Chem. 79 (2007) 2325–2338.
[18] J. Tauchman, G. Süss-Fink, P. Stepnicka, O. Zava, P.J. Dyson, J. Organomet. Chem. 723 (2013) 233–238.
[19] T.M. Sielecki, J.F. Boylan, P.A. Benfield, G.L. Trainor, J. Med. Chem. 43 (1999) 1–18.
[20] Z. Zang, L. Jin, X. Qian, M. Wei, Y. Wang, J. Wang, Y. Yang, Q. Xu, Y. Xu, F. Liu, ChemBioChem. 8 (2007) 113–121.
[21] P.K.M. Siu, D.L. Ma, C.M. Che, Chem. Commun. (2005) 1025–1027.
[22] V. Brabec, O. Nov'akov', Drug Resist. Updates 9 (2006) 111–122.
[23] Z. Xiao-Long, H. Mei-Jiao, Z. An-Guo, W. Ke-Zhi, J. Inorg. Biochem. 107 (2012) 104–110.
[24] M. Barcelo, A. Garcia, A. Terroon, E. Molins, M.J. Prieto, V. Moreno, J. Martinez, V. Llado, I. Lopez, A. Gutierrez, P.V. Escriba, J. Inorg. Biochem. 101 (2007) 649–659.
[25] T.K. Goswami, B.V.S.K. Chakravarthi, M. Roy, A.A. Karande, A.R. Chakravarty, Inorg. Chem. 50 (2011) 8452–8464.
[26] M.N. Patel, C.R. Patel, H.N. Joshi, K.P. Thakor, Spectrochim. Acta Part A 127 (2014) 261–267.
[27] A. Tarushi, K. Lafazanis, J. Kljun, I. Turel, A.A. Pantazaki, G. Psomas, D.P. Kessissoglou, J. Inorg, Biochem. 121 (2013) 53–65.
[28] T. Mosmann, J. Immunol. Methods 65 (1983) 55–63.
[29] A. Arunkumar, M.R. Vijayababu, P. Kanagaraj, K. Balasubramanian, M.M. Aruldhas, J. Arunakaran, Biol. Pharm. Bull. 28 (2005) 740–743.
[30] L. Pejov, V.M. Petrusevski, J. Phys. Chem. Solids 63 (2002) 1873–1881.
[31] J.M. Kelly, A.B. Tossi, D.J. McConnell, Nucleic Acids Res. 13 (1985) 6017–6034.
[32] G. Son, J. Yeo, M. Kim, S. Kim, A. Holmen, B. Akerman, B. Norden, J. Am. Chem. Soc. 120 (1998) 6451–6457.
[33] S. Tabassum, W.M. Al–Asbahy, M. Afzal, F. Manalshamsi, Arjmand, J. Lumin. 132 (2012) 3058–3065.
[34] A.M. Pyle, J.P. Rehmann, R. Meshoyrer, C.V. Kumar, N.J. Turro, J.K. Barton, J. Am. Chem. Soc. 111 (1989) 3051–3058.
[35] G. Zhao, H. Lin, S. Zhu, H. Sun, Y. Chen, J. Inorg. Biochem. 70 (1998) 219–226.
[36] S. Dhar, M. Nethaji, A.R. Chakravarty, J. Inorg. Biochem. 99 (2005) 805–812.
[37] R.F. Pasternack, M. Cacca, B. Keogh, T.A. Stephenson, A.P. Williams, F.J. Gibbs, J. Am. Chem. Soc. 113 (1991) 6835–6840.
[38] J.R. Lakowicz, G. Weber, Biochemistry 12 (1973) 4161–4170.
[39] S. Eriksson, S.K. Kim, M. Kubista, B. Norden, Biochemistry 32 (1993) 2987–2998.
[40] A. Biancardi, T. Biver, F. Secco, B. Mennucci, Phys. Chem. Chem. Phys. 15 (2013) 4596–4603.
[41] A.K. Williams, S.C. Dasilva, A. Bhatta, B. Rawal, M. Liu, E.A. Korobkova, Anal. Biochem. 422 (2012) 66–73.
[42] S. Satyanarayana, J.C. Dabrowiak, J.B. Chaires, Biochemistry 32 (1993) 2573–2584.
[43] D. Suh, J.B. Chaires, Bioorg. Med. Chem. 3 (1995) 723–728.
[44] J.R. Lakowicz, Principles of Fluorescence Spectroscopy, 2nd ed., Plenum Press, New York, 1999.
[45] Y. Wang, H. Zhang, G. Zhang, W. Tao, S. Tang, J. Lumin. 126 (2007) 211–218.
[46] S. Wu, W. Yuan, H. Wang, Q. Zhang, M. Liu, K. Yu, J. Inorg. Biochem. 102 (2008) 2026.
[47] B. Ahmad, S. Parveen, R.H. Khan, Biomacromolecules 7 (2006) 1350–1356.
[48] B. Mishra, A. Barik, K.I. Priyadarsini, H. Mohan, J. Chem. Sci. 117 (2005) 641–647.
[49] C. Tan, S. Hu, J. Liu, J. Liangnian, Eur. J. Med. Chem. 46 (2011) 1555–1563.
[50] G. Tabb, C. Cassino, G. Cavigiolio, D. Colangelo, A. Ghiglia, I. Viano, D. Osella, J. Med. Chem. 45 (2002) 5786–5796.
[51] F. Bao-Li, X. Wu-Shuang, G. Wei-Lin, J. Zhang, Y. Zhao, L. Jian-Ying, C.E. Anson, A. K. Powell, J. Photochem. Photobiol. B 142 (2015) 77–85.
[52] C. Renvoize, A. Biola, M. Pallardy, J. Breard, Cell Biol. Toxicol. 14 (1998) 111–120.